ADVANCED MATERIALS

with these topologies are difficult to fabricate with other lithographic techniques, such as photolithography.[10] Combined with our previous work,[5] which described methods to mold patterned composites of gels, the techniques discussed here allow the formation of structures that incorporate distinct populations of cells within or on the surface of a gel. These lithographic techniques thus enable the formation of micrometer-scale tissues in vitro that contain separate epithelial and mesenchymal compartments.

Experimental

Stamps were cast from patterned lithographic masters using polydimethylsiloxane (PDMS, Sylgard 184, Dow Corning), as described previously [20]. Stamps were coated by adsorption of a monolayer of bovine serum albumin (fatty acid-poor BSA, Calbiochem; 1 % in PBS, > 1 h) to allow distortion-free detachment of molded gels [5]. To fabricate collagen gels with defined cavities, we first added liquid precursors of Matrigel (BD Biosciences; ~ 0.2–0.4 $\mu L\,mm^{-2}$) to the patterned surface of a treated stamp, and centrifuged the stamp (for isolated features, 200 g, 10 min, 4 °C; for interconnected features, 50 g, 5 min, 4 °C) to remove excess liquid Matrigel precursor from the raised regions of the stamp. The stamp was brought vertically into contact with a flat layer (~ 100 μm thick) of collagen gel (rat tail collagen type I, BD Biosciences, 3.66 $mg\,mL^{-1}$; pre-cooled to 4 °C) on a Petri dish or a glass cover slip, and heated to 37 °C at 100 % humidity (40–60 min) to gel the molded Matrigel. We removed the stamp by carefully adding excess PBS; the surface tension of PBS caused the stamp to detach spontaneously from the underlying gels. We then slowly flushed the surrounding PBS with liquid collagen precursors two to three times until the molded Matrigel was completely immersed in liquid collagen precursors; heating the sample to 37 °C at 100 % humidity (30 min) allowed the added collagen precursors to gel and thereby encase the Matrigel. Immersion of the composite of gels in dispase (GIBCO; 2–2.5 $U\,mL^{-1}$ in PBS or culture media, 1.5–2.5 h, 37 °C) digested the Matrigel. The digestion was stopped by washing with fresh PBS or media.

To incorporate iron powder in Matrigel, iron powder (Polysciences, average size of iron particles ~ 10 μm) was coated with BSA (1 %, 1 h), and mixed with liquid Matrigel precursors at ~ 1:5 volume ratio. To incorporate cells in Matrigel, cells were trypsinized, washed with PBS, concentrated by centrifugation (300 g, 2 min), and mixed with liquid Matrigel precursors at ~ 1:2 volume ratio (~ 10^7 $cells\,mL^{-1}$). The iron particles or cells in liquid Matrigel precursors were allowed to settle in the relief features of the stamp (5–10 min, 4 °C) before centrifugation and removal of excess liquid Matrigel precursors. To generate fluorescent features of Matrigel, Alexa Fluor 488-conjugated goat IgG (Molecular Probes, 200 $\mu g\,mL^{-1}$), and Oregon Green 488-conjugated human collagen type IV (Molecular Probes, 250 $\mu g\,mL^{-1}$) were mixed with liquid Matrigel precursors.

Bovine pulmonary artery endothelial cells (BPAECs) (Cambrex BioScience) were cultured in Dulbecco's modified eagle's medium (DMEM) that contained 10 % calf serum (CS, GIBCO). Madin–Darby canine kidney (MDCK) cells (ATCC) were cultured in minimum essential medium that contained 10 % CS. Normal rat kidney (NRK) epithelial cells (ATCC) were cultured in DMEM that contained 10 % fetal bovine serum (GIBCO). Media were supplemented with 1 % penicillin–streptomycin–glutamine (GIBCO). Cells were cultured at 37 °C, 5 % CO_2, and 100 % humidity.

Received: April 15, 2004

[1] X. M. Zhao, Y. N. Xia, G. M. Whitesides, *Adv. Mater.* **1996**, *8*, 837.
[2] M. J. Elices, M. E. Hemler, *Proc. Natl. Acad. Sci. USA* **1989**, *86*, 9906.
[3] D. Kirchhofer, L. R. Languino, E. Ruoslahti, M. D. Pierschbacher, *J. Biol. Chem.* **1990**, *265*, 615.
[4] W. T. Arthur, N. K. Noren, K. Burridge, *Biol. Res.* **2002**, *35*, 239.
[5] M. D. Tang, A. P. Golden, J. Tien, *J. Am. Chem. Soc.* **2003**, *125*, 12 988.
[6] D. J. Beebe, J. S. Moore, J. M. Bauer, Q. Yu, R. H. Liu, C. Devadoss, B. H. Jo, *Nature* **2000**, *404*, 588.
[7] Y. L. Cao, A. Rodriguez, M. Vacanti, C. Ibarra, C. Arevalo, C. A. Vacanti, *J. Biomater. Sci., Polym. Ed.* **1998**, *9*, 475.
[8] H. J. Kong, M. K. Smith, D. J. Mooney, *Biomaterials* **2003**, *24*, 4023.
[9] M. P. Lutolf, J. L. Lauer-Fields, H. G. Schmoekel, A. T. Metters, F. E. Weber, G. B. Fields, J. A. Hubbell, *Proc. Natl. Acad. Sci. USA* **2003**, *100*, 5413.
[10] K. T. Nguyen, J. L. West, *Biomaterials* **2002**, *23*, 4307.
[11] D. A. Wang, C. G. Williams, Q. A. Li, B. Sharma, J. H. Elisseeff, *Biomaterials* **2003**, *24*, 3969.
[12] H. K. Kleinman, M. L. McGarvey, L. A. Liotta, P. G. Robey, K. Tryggvason, G. R. Martin, *Biochemistry* **1982**, *21*, 6188.
[13] K. S. Stenn, R. Link, G. Moellmann, J. Madri, E. Kuklinska, *J. Invest. Dermatol.* **1989**, *93*, 287.
[14] H. K. Kleinman, L. Luckenbill-Edds, F. W. Cannon, G. C. Sephel, *Anal. Biochem.* **1987**, *166*, 1.
[15] H. K. Kleinman, M. L. McGarvey, J. R. Hassell, V. L. Star, F. B. Cannon, G. W. Laurie, G. R. Martin, *Biochemistry* **1986**, *25*, 312.
[16] F. H. Silver, R. L. Trelstad, *J. Biol. Chem.* **1980**, *255*, 9427.
[17] A. Pluen, P. A. Netti, R. K. Jain, D. A. Berk, *Biophys. J.* **1999**, *77*, 542.
[18] J. Vera, R. Alvarez, E. Murano, J. C. Slebe, O. Leon, *Appl. Environ. Microbiol.* **1998**, *64*, 4378.
[19] E. J. Menzel, C. Farr, *Cancer Lett.* **1998**, *131*, 3.
[20] A. Kumar, G. M. Whitesides, *Appl. Phys. Lett.* **1993**, *63*, 2002.

Directed Growth of Ordered Arrays of Small-Diameter ZnO Nanowires**

By *Eric C. Greyson*, *Yelizaveta Babayan*, and *Teri W. Odom**

The controlled growth of optically functional nanometer-scale materials is of importance to several interesting scientific problems. These include two-dimensional (2D) photonic crystals, single-nanowire lasers, and chemical- and light-based sensors.[1–3] The ability to define the position, size, and density of nanostructures on surfaces enables detailed studies of the properties of individual structures and the collective properties of their assemblies. For example, one-dimensional (1D) arrays of equally spaced metallic nanoparticles are predicted

[*] Prof. T. W. Odom, E. C. Greyson, Y. Babayan
Department of Chemistry, Northwestern University
2145 Sheridan Road, Evanston, IL 60208 (USA)
E-mail: todom@chem.northwestern.edu

[**] This work was supported by the Research Corporation, the David and Lucile Packard Foundation, the NASA Institute for Nanoelectronics and Computing, the NSF under Award CHE-0349302, and start-up funds from Northwestern University. We thank Prof. Hupp for use of his UV-vis spectrometer, and Prof. Hui Cao and Xiaohue Wu for use of their PL set-up.

  DOI: 10.1002/adma.200400765

to exhibit extremely narrow (< 10 nm) plasmon resonances compared to individual or disordered arrays of nanoparticles.[4,5] Nanometer-scale fabrication methods are well-suited for manipulating nanostructures on surfaces because the critical feature sizes are nearly of the same magnitude. In particular, soft-lithographic nanopatterning has been used to template the growth of small (20 nm) inorganic salt crystals in periodic arrays of 100 nm wells and to generate feature sizes as small as 30 nm in the photoresist and metal over areas covering 1 in.^{2} (1 in. = 2.54 cm).[6]

ZnO nanostructures have been receiving a considerable amount of attention due to their emission in the near-UV,[1,7,8] strong absorption in the UV,[9] and field-emission capabilities.[10] Previously, ZnO nanowires have been grown on different substrates (e.g., sapphire, silica, silicon) from square micrometer-sized gold patterns using vapor–liquid–solid (VLS) methods. Additionally, the epitaxial growth of ZnO on α-sapphire substrates resulted in well-aligned nanowires.[1,11,12] The catalytic gold areas were generated by the evaporation of gold through masks such as transmission electron microscopy (TEM) grids and monolayers of sub-micrometer spheres.[11,13] Although masks of sub-micrometers spheres can be used to generate gold dots several hundred nanometers in diameter, the patterns are limited to a hexagonal, interconnected honeycomb lattice. We have developed simple nanofabrication techniques that can pattern, in parallel, large numbers of nanostructures at specific locations, with periodic order, variable spacing, and symmetry over areas of ~ 1 cm^2.

Figure 1A summarizes the procedure for generating arrays of small (40–200 nm) gold dots on a substrate, and the subsequent growth of ZnO nanowires from the patterned areas. We generated small features (50–250 nm) in photoresist on a thin (15–20 nm) gold film by phase-shifting photolithography with composite poly(dimethylsiloxane) PDMS masks.[14] These masks were patterned with lines of variable spacing (1–15 μm); this spacing controls the pitch of the patterned features. To fabricate dots in the photoresist having different symmetry and spacing, we performed two consecutive exposures of the positive-tone photoresist: i) through a mask in an initial orientation; and ii) through a mask rotated by an angle θ relative to the orientation of lines in the first exposure step (Fig. 1B). We then subjected the patterned photoresist on the gold film to an isotropic wet etchant, which removed the gold areas that were not protected by the photoresist.[6,15] After dissolution of the resist in acetone, the pattern in the photoresist was transferred into patterns of gold.

We generated circular, catalytic gold areas of small diameters (40–200 nm) in ordered square arrays, hexagonal arrays, and rectangular (nearly 1D) arrays (Fig. 2, insets). Square (hexagonal) lattices of gold dots were generated after etching the photoresist posts that were produced by one exposure via a mask of 2 μm lines spaced by 2 μm, followed by a second exposure of the same mask with $\theta = 90°$ ($\theta = 60°$) (Figs. 2A,B, insets). A mask for the second exposure patterned with 15 μm lines spaced by 15 μm and rotated by $\theta = 90°$ resulted in a quasi-1D lattice (Fig. 2C, inset). Thus; we can pattern different symmetries and spacing of gold dots by i) using masks patterned with variable line spacing; and ii) rotating the mask for the second exposure through an arbitrary angle θ. Besides designing the symmetry and pitch of the gold dots, we can controllably over-etch the metal film to reduce the size of the gold areas.[15] In principle, the sizes of the gold dots can be reduced down to the size of a single gold grain (10–20 nm). One drawback of this size reduction scheme is that wet chemical etchants for metal films are generally isotropic; therefore, obtaining the same sized features under identical etching conditions can be challenging.

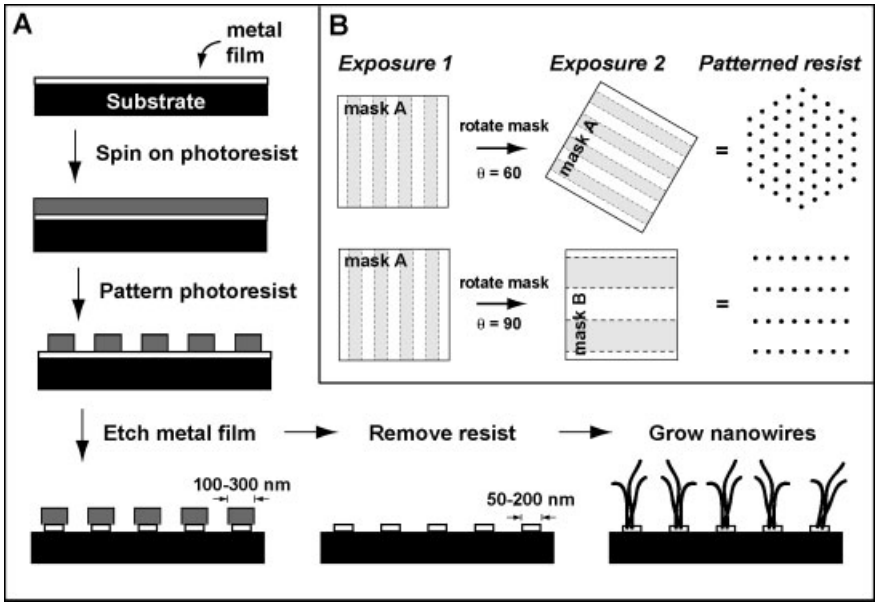

Figure 1. Schematic diagram depicting A) the patterning of catalytic gold dots and the growth of ZnO nanowires and B) the procedure to pattern the photoresist posts with different symmetries and spacing using phase-shifting photolithography. Top–down view of two exposures through phase-shifting masks to generate dots in positive-tone resist having hexagonal and rectangular symmetry. The dashed lines and gray areas indicate the recessed regions of the PDMS mask.

Small diameter ZnO nanowires were grown from patterned, thin gold dots on sapphire substrates using a vapor–liquid–solid (VLS) process. The source materials, ZnO and graphite powders, were ground and placed inside and off-center in a quartz tube furnace, which was held at 900 °C, while the substrate was placed far downstream (beyond the heating coils of the furnace). Growth of the ZnO nanowires from the gold sites occurred in a relatively cool zone, with temperatures ca. 600 °C.

Scanning electron microscopy (SEM) images revealed arrays of ZnO nanowires grown on the patterned gold dots

ADVANCED MATERIALS

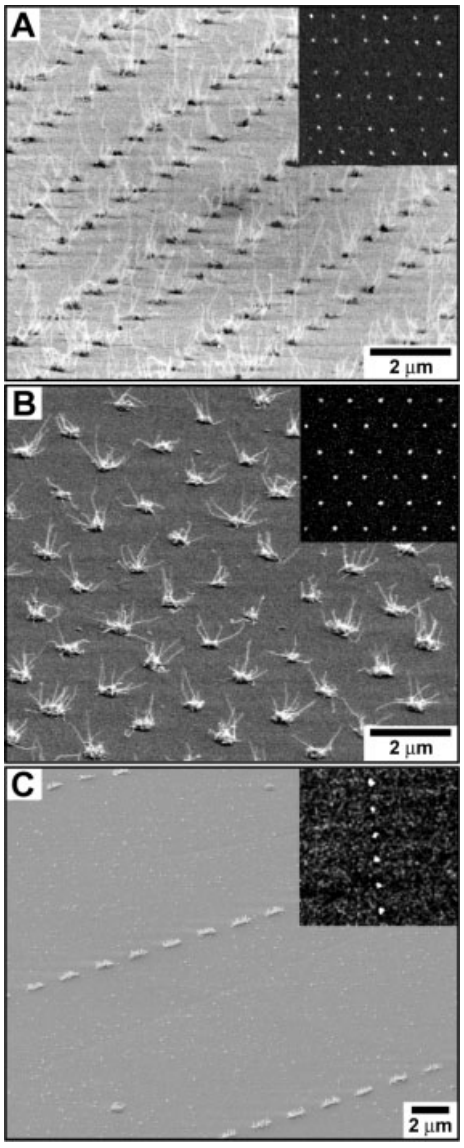

Figure 2. SEM images of arrays of ZnO nanowires grown from the gold dots. A) Square lattice imaged with a tilt of 80°. B) Hexagonal lattice imaged with a tilt of 63°. The base from which the ZnO nanowires grow is much larger than the diameter of the patterned gold dots. Because we are growing in a cool zone, this base is most likely a combination of amorphous ZnO and gold. C) Rectangular lattice imaged with a tilt angle of 45°. Adjacent gold dots merged together in the ZnO growth process, which explains why the short (1–2 μm) ZnO nanowires appear to grow from elongated dots. Insets: SEM images of gold patterned in different symmetries and spacing. The lateral size of the gold dots ranged between 50–200 nm. The inset areas are 12 μm × 12 μm.

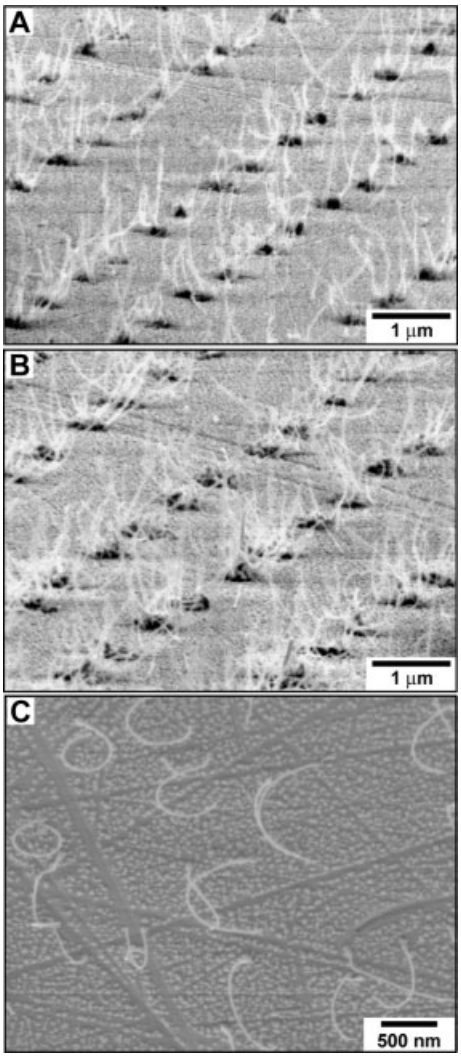

Figure 3. SEM images of arrays of ZnO nanowires grown from A) small (50–100 nm) gold dots and B) large (150–200 nm) gold dots. C) SEM image of isolated nanowires that bend over (in less than 10 s) under imaging conditions of a 3 keV electron beam.

(Fig. 2). Arrays of nanowires grew in square, hexagonal, and 1D lattices; the ZnO nanowires exhibited different lengths depending on the growth conditions. Figures 3A,B show that smaller gold dots (50–100 nm) directed the growth of small numbers (3–10) of ZnO nanowires, whilst the larger gold dots (150–200 nm) initiated the growth for increased numbers (15–20) of ZnO nanowires. Despite the different sizes of the gold dots, the nanowires extending from the dots have diameters similar in size. These nanowires are very narrow in diameter (10–15 nm), are relatively long in length (2–10 μm), and often exhibit slight curvature. We attribute this curvature to their high aspect ratios (~1:1000) and small diameters. A single gold dot does not appear to direct the growth of a single nanowire; upon heating, the patterned dot breaks into a cluster of small gold droplets, which initiates the growth of the thin nanowires. Because many of these small gold droplets are no longer at the surface of the sapphire substrate, the nanowires do not grow epitaxially to and perpendicular to the surface. In addition, under exposure of low electron energies (~3 keV), these small diameter nanowires appear quite flexible and can be induced to bend onto the substrate. We observed this behavior for multiple nanowires that were grown from an individual gold dot and for isolated wires that were grown on residual gold areas that were left on the surface after imperfect etching (Fig. 3C).

To characterize the crystallinity of the nanowires by transmission electron microscopy (TEM), we removed the wires from the patterned substrate by ultra-sonication in ethanol. Figures 4A,B depict high-resolution transmission electronmicroscopy (HRTEM) images of individual ZnO nanowires. We observed nanowire growth primarily along the [001] direction for curved and straight nanowires. In Figure 4A, the (100) planes with lattice spacing of 2.8 Å are visible and orthogonal to the growth direction of the nanowire; Figure 4B shows a

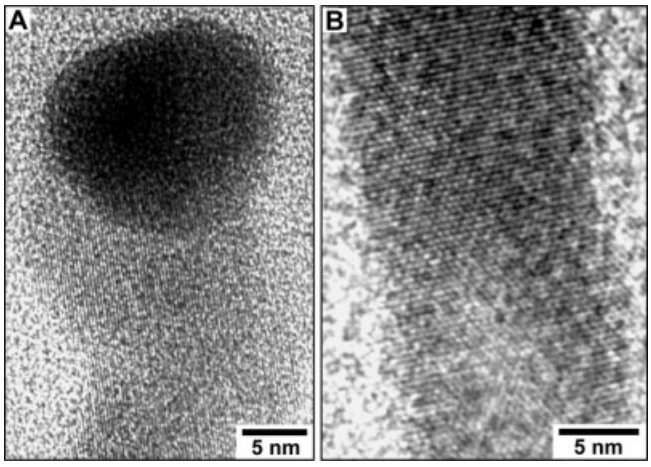

Figure 4. High-resolution TEM images of A) a gold dot at the end of a curved ZnO nanowires, and B) lattice-resolved image of a straight ZnO nanowire. Growth occurs along the [001] direction.

hexagonal lattice with a spacing of 3.9 Å, between the (003) planes, along the growth direction. For all of the nanowires that we characterized, a catalytic gold particle was found attached to one end of the crystalline ZnO nanowire.

We have measured the optical properties of these patterned ZnO nanowire arrays from UV-visible absorption and photoluminescence (PL) measurements. The PL of ordered ZnO nanowire arrays was measured using a He–Cd laser (325 nm) as the excitation source. Figure 5 shows strong room-temperature emission[8] ~374 nm for the arrays of ZnO nanowires arranged in a square lattice pattern. The narrow (15 nm) full

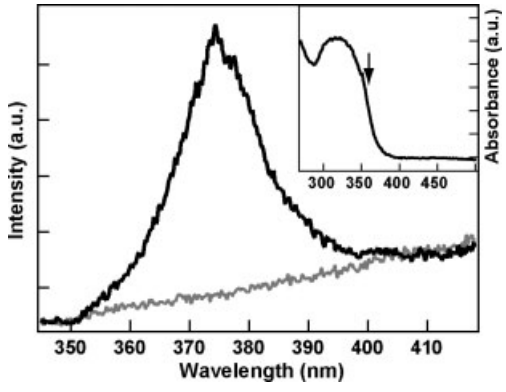

Figure 5. Photoluminescence spectrum acquired from arrays of ZnO nanowires patterned in a square lattice. Inset: UV-vis absorption spectrum. The arrow indicates the absorption band edge.

width at half maximum PL peak is another indication of the uniformity of diameters in the arrays of ZnO nanowires. In addition, because of the small diameters of our ZnO nanowires, the edge of the absorption band (Fig. 5, inset) is shifted towards a shorter wavelength (~355 nm) compared to other ZnO nanorods.[16,17]

The advantages of applying our soft-lithographic techniques to the growth of ordered, functional materials include: i) patterned areas with features of variable symmetry and spacing; ii) periodic arrays over large areas (1 in.^{2}); and iii) patterns generated in a single patterning step. One disadvantage of our technique is that the pitch of the structures is determined by the resolution of the chrome masks that are used in order to fabricate the PDMS stamps, which is limited to ~500 nm. Other types of lithography, such as electron-beam lithography and scanning-probe lithographies, can be used for patterning small gold dots with different symmetries and spacing. These methods, however, are serial techniques that are limited to patterning over small (10–100 μm) areas in a single writing step.

In summary, we have demonstrated how simple nanofabrication techniques can be used to generate catalytic patterns for the directed growth of optically functional and crystalline nanomaterials. These patterns can be fabricated in parallel, with different symmetries and pitch, and over large areas. Because we can control the spacing and symmetry of the patterned catalytic areas, we can investigate how light interaction between neighboring nanowires affects collective properties.[18] Our patterning methods, moreover, are used as a general approach that can be applied to the growth of other types of nanometer-scale materials from catalytic dots of different metals and have potential for patterning isolated and individual nanostructures. Such flexibility can foster new opportunities in photonic-based applications for wavelengths from the UV to near-IR for arrays of nanometer-scale light sources and detectors.

Experimental

Fabrication of Arrays of Gold Dots: We deposited a thin (15–20 nm) metal film of gold by electron-beam evaporation on clean sapphire (110) substrates (Valley Design). We generated two-dimensional arrays of posts (50–200 nm in diameter) in Shipley 1805 photoresist by phase-shifting photolithography [14]. Two different exposures were performed through masks patterned with lines and spacings between 1–15 μm. These patterned posts protected the underlying gold areas when subjected to an isotropic wet etchant (Transene type TFA), diluted 1:2 with water. After the patterned substrates were etched for 6–8 s, the pattern in the photoresist was transferred into gold.

Growth of Arrays of ZnO Nanowires: Sapphire substrates with patterned Au dots were placed in a 2 in. diameter tube furnace whose center temperature was held at 900 °C. The substrates were placed far downstream (3–4 in.) from an alumina boat filled with 0.3 g ZnO, 0.6 g carbon under a flow of 100 sccm Ar.

Characterization of Arrays of ZnO Nanowires: SEM images of ZnO nanowires were obtained on a LEO 1525 (samples were sputtered with Pt/Pd to reduce charging from the substrate). TEM images were acquired using a Hitachi HF-2000. Absorption spectra were measured using a Cary 5000 spectrometer. For the room-temperature

ADVANCED MATERIALS

PL, a continuous wave (cw) He–Cd laser (325 nm) with an output power of 20 mW was used as the excitation source. The PL was dispersed through a SPEX Triax 500 spectrometer with a 600 lines/mm grating and was detected by a nitrogen-cooled charge-coupled device (CCD) camera.

Received: April 15, 2004

[1] M. Huang, S. Mao, H. Feick, H. Yan, Y. Wu, H. Kind, E. Weber, R. Russo, P. Yang, *Science* **2001**, *292*, 1897.
[2] K. Kempa, B. Kimball, J. Rybczynski, Z. P. Huang, P. F. Wu, D. Steeves, M. Sennett, M. Giersig, D. V. G. L. N. Rao, D. L. Carnahan, D. Z. Wang, J. Y. Lao, W. Z. Li, Z. F. Ren, *Nano Lett.* **2003**, *3*, 13.
[3] X. Feng, L. Feng, M. Jin, J. Zhai, L. Jiang, D. Zhu, *J. Am. Chem. Soc.* **2004**, *126*, 62.
[4] S. Zhou, L. Zhao, G. C. Schatz, *Proc. SPIE-Int. Soc. Opt. Eng.* **2003**, *5221*, 174.
[5] S. Malynych, G. Chumanov, *J. Am. Chem. Soc.* **2003**, *125*, 2896.
[6] T. W. Odom, V. R. Thalladi, J. C. Love, G. M. Whitesides, *J. Am. Chem. Soc.* **2002**, *124*, 12 112.
[7] Z. K. Tang, G. K. L. Wong, P. Yu, M. Kawasaki, A. Ohtomo, H. Koinuma, Y. Segawa, *Appl. Phys. Lett.* **1998**, *72*, 3270.
[8] Y. C. Kong, D. P. Yu, B. Zhang, W. Fang, S. Q. Seng, *Appl. Phys. Lett.* **2001**, *78*, 407.
[9] E. A. Meulenkamp, *J. Phys. Chem. B* **1998**, *102*, 5566.
[10] C. Liu, J. A. Zapien, Y. Yo, X. Megn, C. S. Lee, S. Fan, Y. Lifshitz, S. T. Lee, *Adv. Mater.* **2003**, *15*, 838.
[11] P. Yang, Y. Haoquan, S. Mao, R. Russo, J. Johnson, R. Saykally, N. Morris, J. Pham, R. He, H.-J. Choi, *Adv. Funct. Mater.* **2002**, *12*, 323.
[12] M. Huang, Y. Wu, H. Feick, N. Tran, E. Weber, P. Yang, *Adv. Mater.* **2001**, *13*, 113.
[13] X. Wang, C. J. Summers, Z. L. Wang, *Nano Lett.* **2004**, *4*, 423.
[14] T. W. Odom, J. C. Love, K. E. Paul, D. B. Wolfe, G. M. Whitesides, *Langmuir* **2002**, *18*, 5314.
[15] J. C. Love, K. E. Paul, G. M. Whitesides, *Adv. Mater.* **2001**, *13*, 604.
[16] B. Liu, H. C. Zeng, *Langmuir* **2004**, *20*, 4196.
[17] J.-J. Wu, S.-C. Liu, *J. Phys. Chem. B* **2002**, *106*, 9546.
[18] A. L. Burin, H. Cao, G. C. Schatz, M. A. Ratner, *J. Opt. Soc. Am. B* **2004**, *21*, 121.

Electroactive Substrates that Reveal Aldehyde Groups for Bio-Immobilization**

By *Woon-Seok Yeo* and *Milan Mrksich**

The development of surfaces that have switchable properties offers a new dimension in the design of advanced materials.[1–5] For biological applications, the recent development of surfaces that allow the modulation of ligand activity, protein immobilization, and cell adhesion has enabled studies of cell–cell communication, provided routes to engineered tissue, and is motivating the design of hybrid microsystems that integrate cells as functional components.

Our approach to dynamic substrates has emphasized the design of self-assembled monolayers that respond to applied potentials by modulating the activities of immobilized ligands.[6–12] Our strategy is based on monolayers that can be switched to initiate the selective immobilization of a ligand. An earlier example from our laboratory used an electrochemical oxidation of hydroquinone to benzoquinone, which then participates in a Diels–Alder reaction with a diene-tagged ligand to immobilize the ligand.[6,8,10] While this scheme benefits from a rapid and very selective immobilization reaction, it does require the synthesis of a diene-tagged ligand. To generate an analogous strategy that can be used for the immobilization of a variety of unmodified proteins and ligands, we report here a surface that reveals an aldehyde functionality in response to an oxidative potential, and which allows immobilization of amino-functionalized ligands.

Our approach begins with a self-assembled monolayer (SAM) on gold that presents a 4-*H*-benzo[*d*][1,3]dioxinol group.[13] The acetal functionality in this molecule masks an aldehyde functional group. Application of an oxidative potential to the monolayer causes the oxidation of the aromatic ring with hydrolysis of the acetal to yield the corresponding aldehyde group. The resulting aldehyde can be used in several formats for immobilizing ligands, including condensation with hydrazide-tagged ligands (Fig. 1). In this paper, we demonstrate a monolayer having this dynamic property and illustrate its use by first immobilizing a ligand and subsequently immobilizing a corresponding protein to the ligand. Further, we show this dynamic substrate can be applied to studies of cell migration.

We used cyclic voltammetry to characterize the electrochemical conversion of the protected aldehyde. We first pre-

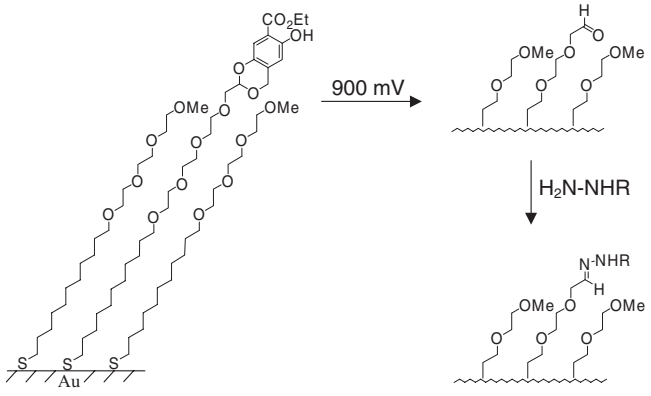

Figure 1. Strategy for preparing a dynamic substrate that reveals aldehyde groups. A monolayer presenting the 4-*H*-benzo[*d*][1,3]dioxinol group is subjected to an electrical potential at 900 mV to yield an aldehyde group. This group reacts with hydrazide-tagged ligands to give immobilization of the ligand by way of a hydrazone linkage.

[*] Prof. M. Mrksich, Dr. W.-S. Yeo
Department of Chemistry and Institute for Biophysical Dynamics
The University of Chicago
5735 S. Ellis Ave., Chicago, IL 60637 (USA)
E-mail: mmrksich@uchicago.edu

[**] This work was supported by the National Science Foundation and the Army Research Office.

  DOI: 10.1002/adma.200400591